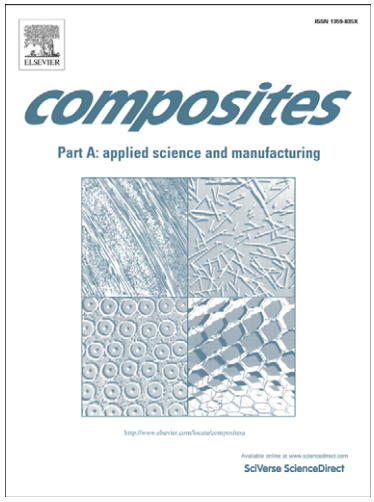

Modelling the viscoelastic stress relaxation of glass fibre reinforcements under constant compaction strain during composites manufacturing

A.A. Somashekar, S. Bickerton, D. Bhattacharyya

PII: S1359-835X(12)00053-X
DOI: 10.1016/j.compositesa.2012.02.004
Reference: JCOMA 3109

To appear in: *Composites: Part A*

Received Date: 3 October 2011
Revised Date: 2 February 2012
Accepted Date: 4 February 2012

Please cite this article as: Somashekar, A.A., Bickerton, S., Bhattacharyya, D., Modelling the viscoelastic stress relaxation of glass fibre reinforcements under constant compaction strain during composites manufacturing, *Composites: Part A* (2012), doi: 10.1016/j.compositesa.2012.02.004

Modelling the viscoelastic stress relaxation of glass fibre reinforcements under constant compaction strain during composites manufacturing

A. A. Somashekar, S. Bickerton and D. Bhattacharyya*

Centre for Advanced Composite Materials,

Department of Mechanical Engineering, The University of Auckland,

Private Bag 92019, Victoria Street West, Auckland 1142, New Zealand.

ABSTRACT

Viscoelastic stress relaxation of glass fibre reinforcements is commonly encountered in the manufacture of glass fibre reinforced polymer composites. A better understanding of the phenomenon, coupled with an ability to predict this behaviour, will aid improved manufacturing process control and tooling design. Finished product quality may also be bettered by virtue of increased knowledge of stresses acting within the composite product. This paper presents a simple Maxwell element-based model to both simulate and help explain the viscoelastic stress relaxation of glass fibre reinforcements under compressive strain compaction of layers during composites manufacturing. The model was validated against experimental data for reinforcement materials of different architecture, and good-to-reasonable predictions of the stress relaxation response were obtained.

Keywords: A. Glass fibres B. Stress relaxation C. Analytical modelling Not in list.

* Corresponding author. Tel: +64 9 923 8149; fax: +64 9 373 7005.
Email address: d.bhattacharyya@auckland.ac.nz (D. Bhattacharyya).

Maxwell element-based model

1. Introduction

Glass fibre reinforcements of varied architecture are commonly used in the manufacture of composite parts for different applications in industries as diverse as automotive, marine, aerospace, infrastructure and sports goods. These reinforcements are generally compacted during composites manufacturing in order to achieve the desired fibre volume fraction within the thickness of the manufactured product. The finished article is the compacted reinforcement infused and encased within a cured polymeric resin matrix that has the required shape, size and colour of the final product. Liquid composite moulding (LCM) processes are often employed for composites manufacturing, and this research is based on LCM methodology. However, several other methods also exist for making glass fibre reinforced polymer (GFRP) composites. Whatever the method is, it is usually necessary to compress the reinforcement to the required thickness at the start of and sometimes also during the manufacturing process. In some cases the reinforcement is compacted to a given stress, rather than to a given final thickness. In any case, the compressed reinforcement is often held at that reduced or final thickness for some period of time while the next step in the manufacturing process get underway. During this period the reinforcement undergoes viscoelastic stress relaxation. The objective of this study was to understand this phenomenon, and to develop and build a simple model to help explain and simulate the experimentally observed stress relaxation behaviour of four very different types of commonly used glass fibre reinforcements. The materials studied were Biaxial Stitched (Non-Crimp) Fabric (BSF), Chopped Strand Mat (CSM), Continuous Filament Mat (CFM) and Plain Weave Fabric (PWF).

Sample images of these materials are presented in Fig. 1, while Table 1 lists their specifications. It is envisaged that increased understanding of stress relaxation will facilitate better die, mould and tooling design by virtue of greater knowledge of forces and stresses acting on and within them. In addition, finished product quality may also be enhanced as a result of increased awareness of stresses acting within the reinforcement.

Research on compaction behaviour of glass fibre reinforcements has been reported by other workers such as Kim et al. [1] with E-glass plain weave and random mat reinforcements, Pearce and Summerscales [2] with PWF E-glass reinforcements, and Robitaille and Gauvin [3] with non-crimp bidirectional glass fabric. Two of the present authors reported their initial research on glass fibre compaction response in [4], and these findings corroborate the results in [1-3]. Subsequent work [5-7] considered the types of compression deformation that occur, on quantifying the different components and on visualising and analysing the mechanisms of deformation. In modelling work, Maxwell elements or various combinations thereof can be used to represent viscoleastic stress relaxation under constant compressive strain [8-10]. A Maxwell element consists of a linear (Hookean) spring and a linear viscous dashpot (containing a Newtonian fluid) in series. Kim et al. [1] utilised a model containing five Maxwell elements in parallel (known as the Maxwell-Wiechert model) to simulate stress relaxation after compression of various dry reinforcements, including E-glass plain weave cloth and random mat. They reported that the model provided a good fit to experimental results. More recently, a viscoelastic model to characterise the compression deformation behaviour of fibrous reinforcements in liquid composite moulding processes was developed by Kelly et al. [11]. A free spring in parallel with ‘N’ Maxwell elements was

used to represent both compaction and relaxation phases. They found that a model with one spring and a Maxwell element in parallel showed good agreement with experimental results from compression tests on Continuous Filament Mat reinforcements in both dry and wet states. Following that, Penneru et al. [12, 13] employed a three component Maxwell element-based model (one Maxwell element with a spring in parallel) to satisfactorily describe viscoelastic stress relaxation in wood. Other researchers such as [14, 15] have also employed Maxwell models to simulate stress relaxation and validated them using their experimental data, but the details are not readily apparent from the published results. There is thus a need for a model to adequately describe the stress relaxation response of a variety of glass fibre reinforcement materials, and this paper seeks to address that.

2. Experimental Work

The basic viscoelastic stress relaxation experiment was to compact a reinforcement consisting of a set number of layers (plies) between two flat platens at a constant compression speed, until a preset final thickness was reached. At that point the two platens were held at their respective positions for a pre-determined period of time (i.e. the compressive strain of the reinforcement was held constant). The material underwent viscoelastic stress relaxation during this period, with the compressive load initially dropping off rapidly from its peak value at the start of stress relaxation, and then decreasing more gradually. If a sufficiently long time interval is allowed, it can be seen that the load finally reaches a steady-state plateau or long term value.

The present experimental study explored the stress relaxation behaviour under

compressive strain of BSF, CSM, CFM and PWF at varying compaction levels (i.e. compaction to different final fibre volume fractions or thicknesses). The details of the experimental parameters and results are given in Table 2. The reinforcement types selected for this study are commonly used in industry and are of very different architecture to one another. In each case a range of final fibre volume fractions was chosen, varying from low to high, keeping in mind the maximum pressures being generated and the highest fibre volume fractions generally reached in practice. With regard to the other experimental parameters, a basic guideline to use mid-range values was employed. An Instron Universal Testing Machine (load frame model # 1186, controller model # 5500R, load cell capacity 200 kN static load, auto-ranging) was used for the tests. The machine was controlled using Merlin software (Instron Main Programme version 5.04). A new, untested sample was used for each test.

The viscoelastic stress relaxation behaviour of BSF is discussed here, and is in general, also representative of the stress relaxation response of the other three materials. Fig. 2 shows the results of the BSF tests. It can be noted from Fig. 2a that the peak compression stress increased as the final fibre volume fraction increased, and that the loading path was very similar in all cases. There is a quick reduction in compression stress at the start of the relaxation period, and this tapers off over time, tending towards an asymptotic value after a long period. As the final fibre volume fraction increases, the amount of stress relaxation decreases and more stress remains as final stress (or long term stress), as can be noted from Fig. 2b. This can also be viewed in terms of absolute values of peak and final stresses, as presented in Fig. 2c. It can thus be seen that, in general, with increasing fibre volume fraction, a greater percentage of the peak stress is

retained as final stress (Table 2). As the final fibre volume fraction is increased, free space within the specimen is reduced. It is surmised that there is thus less room for fibre/bundle re-alignment or fibre network re-organisation to take place, this being necessary for stress relaxation. The density of packing of fibres and fibre bundles increases as the final fibre volume fraction is increased, and this in turn constrains the internal movement of fibres and fibre bundles, lowering capacity for stress relaxation. Hence greater stress retention is observed.

3. Viscoelastic Stress Relaxation Model

The model being presented here is based on the Maxwell element. The governing equations for the linear spring (equation 1) and linear viscous dashpot (equation 2) are as follows:

$$\sigma = E\varepsilon_s \tag{1}$$

where σ is the applied stress, E is the spring stiffness and ε_s is the strain.

$$\sigma = \eta \frac{d\varepsilon_d}{dt} \tag{2}$$

Where η is the viscosity coefficient of the fluid in the dashpot and $(d\varepsilon_d/dt)$ is the strain rate.

In a Maxwell element the total strain and the total strain rate are the sums of the individual strains and strain rates respectively, while the stress acting on the two components is the same since they are connected in series.

$$\varepsilon = \varepsilon_s + \varepsilon_d$$

(3) $$\frac{d\varepsilon}{dt} = \frac{d\varepsilon_s}{dt} + \frac{d\varepsilon_d}{dt}$$

(4)

Differentiating equation (1) and substituting it and equation (2) into equation (4) gives

$$\frac{d\varepsilon}{dt} = \frac{1}{E}\frac{d\sigma}{dt} + \frac{1}{\eta}\sigma \tag{5}$$

When a Maxwell element is under constant compaction strain, (dε/dt) is zero. Therefore

$$\frac{1}{E}\frac{d\sigma}{dt} = -\frac{1}{\eta}\sigma \tag{6}$$

Rearranging this gives

$$\frac{d\sigma}{\sigma} = -\frac{E}{\eta}dt \tag{7}$$

Integrating equation (7) results in

$$\ln\sigma = \left(-\frac{Et}{\eta}\right) + C \tag{8}$$

Hence

$$\sigma = \exp\left[\left(-\frac{Et}{\eta}\right) + C\right] = \exp\left(-\frac{Et}{\eta}\right) * \exp[C] \tag{9}$$

At t = 0, $\sigma = \sigma_{max}$; therefore $\exp[C] = \sigma_{max}$

Thus,

$$\sigma(t) = \sigma_{(max)} \exp(-Et/\eta) \tag{10}$$

Equation (10) can be re-written as

$$\sigma(t) = \sigma_{(max)} \exp(-t/\tau) \tag{11}$$

by defining a relaxation time constant τ, which is equal to (η/E).

If a number of Maxwell elements are connected in parallel, the total applied load is distributed across these elements. Trials were conducted with the three component Maxwell element-based model (one Maxwell element with a spring parallel to it, Equation 12) and a double Maxwell element model (two Maxwell elements in parallel, Equation 13), but these were found to be inadequate to describe the stress relaxation

behaviour of the glass fibre reinforcements under consideration.

$$\sigma(t) = \sigma_0 + \sigma_1 \exp(-t/\tau_1) \quad (12)$$

$$\sigma(t) = \sigma_1 \exp(-t/\tau_1) + \sigma_2 \exp(-t/\tau_2) \quad (13)$$

Here σ_0, σ_1 and σ_2 are stress constants, while τ_1 and τ_2 are the relaxation time constants. An example plot from the three component Maxwell element-based model trial is shown in Fig. 3a. It can be seen that this model provides a poor fit in these cases. The double Maxwell model too did not give a good representation of the experimental stress relaxation data.

In the present study, a five component Maxell element-based model (two Maxwell elements and a spring, all in parallel to one another) was however found to provide excellent representation. A schematic diagram of the model is shown in Fig. 3b. The physical explanation of this model and its applicability to the research are discussed in Section 3.1. The evolution of stress with time in the case of the five component Maxwell element-based model is as described by Equation (14):

$$\sigma(t) = \sigma_0 + \sigma_1 \exp(-t/\tau_1) + \sigma_2 \exp(-t/\tau_2) \quad (14)$$

σ_0, σ_1 and σ_2 are the stress constants for the spring and two Maxwell elements respectively, while τ_1 and τ_2 are the relaxation time constants for the two Maxwell elements alone. τ_1 and τ_2 are equal to (η_1/E_1) and (η_2/E_2) respectively.In physical terms, σ_0 is the long term stress that is retained after stress relaxation is complete, while $(\sigma_0+\sigma_1+\sigma_2)$ is equal to $\sigma_{(max)}$, which is the peak stress. (This is the starting stress, which is at time t=0).

3.1. Model Applicability to Experimental Data

σ_0 is less than or equal to the minimum stress in the test data, while $(\sigma_1+\sigma_2)$ is equal to $[\sigma_{(max)} - \sigma_0]$. σ_1 is greater than σ_2 while τ_1 is very much smaller than τ_2, as will be explained later on. These guidelines were used to determine the initial values of these five parameters (σ_0, σ_1, σ_2, τ_1 and τ_2) by trial and error as a first approximation, and the trial-fit model and experimental stress-time curves plotted using Microsoft Excel to check quality of fit. Very good fits were obtained by this method. The initial values of the five parameters thus determined, and the corresponding experimental stress-time data, were then input into MATLAB to determine the best-fit model values of these constants (Table 3). The authors did experiment with inputting different initial values of the five parameters into MATLAB, and the best-fit values output by the code varied only slightly. It can safely be stated that the model parameter values presented in Table 3 are perhaps the best representative figures, and that other combinations of values centred around these numbers would also provide reasonable-to-good fits. A representative trial-fit model curve for Biaxial Stitched Fabric and the corresponding best-fit model curve are shown in Figs. 4a and 4b respectively. This technique was employed for all the four reinforcement materials in this research. The normalised experimental and model stresses as output by MATLAB are given in Table 4. The experimental stress values were normalised with respect to the peak stress in every case. Sample normalised experimental stress versus time graphs along with their best-fit model plots for Chopped Strand Mat, Continuous Filament Mat and Plain Weave Fabric are shown in Fig. 5.

It can be seen from Figs. 4-5 and Table 4 that the five component Maxwell element-based model simulates extremely well the stress relaxation paths of these four

reinforcing materials. In general, as the final fibre volume fraction is increased, the peak compression stress increases. This is due to fibres being compacted to smaller thicknesses, leading to greater resistance. At the same time stress relaxation reduces due to fibre movement becoming more constrained. The model simulation improves as the final fibre volume fraction increases, as can be seen with the results of CFM, CSM and PWF. In the case of BSF all four simulations are more or less equally good. It can be noted that the five component Maxwell-based model under-predicts the peak stress (usually by a small percentage) while minimising the residual value.

When these reinforcements are compressed, the applied compaction stress causes substantial deformation of the reinforcement. Once the final fibre volume fraction (i.e. final sample thickness) is reached and the final compaction strain is held constant, the compression load drops off quickly as no further deformation is imposed on the specimen. Some permanent strain of the specimen would have already occurred, and the compaction load is sustained only by the elastic and viscoelastic strains contained within the sample. The viscoelastic strain is converted to elastic strain over time, depending on the availability of space within the sample for fibre/fibre bundle movement, and hindrance to this realignment by the locations of other fibres and fibre bundles. In an ideal case, all viscoelastic strain would thus become elastic strain over a long period of time. This process results in a corresponding slow reduction in compression stress over time. At the end of stress relaxation, elastic strain still remains and resists the compaction load.

It is explained that σ_1 and τ_1 represent the Maxwell element that corresponds to the

sudden and large drop in compaction stress at the start of the constant compressive strain holding time. The slow and gradual reduction in compression stress due to fibre and fibre bundle reorganisation is represented by the other Maxwell element and its parameters σ_2 and τ_2. σ_1 values are large, compared to σ_2. By the same token, τ_1 is very much smaller than τ_2. τ_1 represents the initial quick drop in stress while τ_2 is so much greater as a result of the slow stress relaxation that occurs over a long period of time. σ_0 is the elastic stress that remains when the steady state plateau is reached.

3.2. Variation of Model Parameters with Fibre Volume Fraction

Figs. 6-9 show the variation of the best-fit values of the five model parameters (σ_0, σ_1, σ_2, τ_1 and τ_2) against the final fibre volume fraction for the four reinforcement materials tested. It is known from experiments and also as noted from Fig 2c that both peak compaction stress and long term stress vary exponentially with fibre volume fraction. As the parameter σ_0 represents the long term stress, an exponential fit was employed for the curve depicting the variation of σ_0 with final fibre volume fraction. The other four parameters (σ_1, σ_2, τ_1 and τ_2) were fitted using second degree polynomial curves. The value of R^2 is equal to or greater than 0.92 in all cases but one, indicating good fits. The lone exception is the variation of σ_0 with final fibre volume fraction in the case of BSF where the R^2 value is 0.81.

3.3 Model Validation

In the present study, two example stress relaxation predictions for Biaxial Stitched Fabric have been made, and compared to the corresponding experimental results (BSF 2, $v_f = 0.55$ and BSF 5, $v_f = 0.625$, Table 2). The comparisons are shown in Figs. 10a

and 10b respectively. It is noted that the predicted curves are very close to the experimental curves, indicating good prediction by the model. The predicted peak stresses are slightly lower than the normalised experimental peak stresses, as in the case of the four BSF tests used for model development (best-fit model curves versus experimental curves). The $\Sigma residual^2$ values are also similar to those obtained with the four BSF tests.

The current model was developed based on the experimental parameters chosen for this study and the test results obtained. Thus model validation with BSF results was against test data using the same set of experimental parameters. However, it would still be useful to test this model in other cases which have different experimental parameters. With this in mind, the model was applied to a CFM test (CFM 5) and a PWF test (PWF 5), both tests (Table 2) having different experimental parameters to those employed in model development. The plots of the corresponding experimental and predicted curves are presented in Figs. 11a and 11b respectively. It can be seen from the figures that the model over-predicts stress relaxation in both cases, and that the variation with the actual experimental curves is greater. Nevertheless, the model presents a good first approximation in both scenarios.

In general terms, this model presents a methodology to successfully simulate, explain and predict viscoelastic stress relaxation. While the fibre volume fraction is a key factor that influences compression stress, other parameters such as compression speed, number of layers and dry/wet state of the reinforcement also affect the compaction load required to reach a certain fibre volume fraction or final thickness. The present model needs to be

improved upon to take account of these other factors. An enhanced model should also incorporate a material type parameter to account for different compaction behaviours exhibited by reinforcements of various architecture or architectural types. The intention is that an expanded version of this model can be quickly developed by conducting a limited number of experiments but be employed to predict the stress relaxation response of a material under a wide variety of manufacturing parameters.

4. Concluding Remarks

It was shown that the five component Maxwell element-based model can be used to obtain good simulations of the stress relaxation response under constant compressive strain of Continuous Filament Mat, Chopped Strand Mat, Plain Weave Fabric and Biaxial Stitched Fabric. The variation of stress constant σ_0 with final fibre volume fraction was fitted with an exponential curve while second degree polynomial curves were used to fit the variations of the other model parameters with final fibre volume fraction. The model was then used to predict the stress relaxation behaviour of Biaxial Stitched Fabric in two cases with the same experimental parameters, in both of which the experimental results were simulated extremely well. When the model was applied to predict the stress relaxation response in CFM and PWF with other test parameters, it over-predicted the relaxation. The model needs to be expanded to account for factors such as compaction speed, number of layers and dry/wet state of the reinforcement.

It is known that natural variation in reinforcement materials exists, leading to differences in compaction response from different samples of the same material. This is even more in the case of materials where stacking and nesting or the presence of

significant binder can affect compression behaviour. Increasing the fibre volume fraction generally leads to higher peak compaction stress, more so at high fibre volume fractions, where even small increases in fibre volume fraction can cause the peak compaction stress to increase considerably. Keeping this knowledge in the background, it can be concluded that the five component Maxwell element-based model can be employed to both simulate and obtain good predictions of the stress relaxation response of these reinforcement materials over a range of fibre volume fractions, keeping other test factors constant.

Acknowledgements

The authors thank the New Zealand Foundation for Research, Science and Technology for funding this research. They would also like to acknowledge the contributions of Dr Sourish Banerjee, Dr Anjaneya Prasad Penneru, Mr Michael J Buntain and technical staff.

References

[1] Kim YR, McCarthy SP, Fanucci JP. Compressibility and relaxation of fiber reinforcements during composite processing. Polymer Composites 1991;12(1):13-19.

[2] Pearce N, Summerscales J. The compressibility of a reinforcement fabric. Composites Manufacturing 1995;6(1):15-21.

[3] Robitaille F, Gauvin R. Compaction of textile reinforcements for composites manufacturing. I: Review of experimental results. Polymer Composites 1998;19(2):198-216.

[4] Bickerton S, Buntain MJ, Somashekar AA. The viscoelastic compression behavior

of liquid composite molding preforms. Composites Part A: Applied Science and Manufacturing 2003;34(5):431-444.

[5] Somashekar AA, Bickerton S, Bhattacharyya D. An experimental investigation of non-elastic deformation of fibrous reinforcements in composites manufacturing. Composites Part A: Applied Science and Manufacturing 2006;37(6):858-867.

[6] Somashekar AA, Bickerton S, Bhattacharyya D. Exploring the non-elastic compression deformation of dry glass fibre reinforcements. Composites Science and Technology 2007;67(2):183-200.

[7] Somashekar AA, Bickerton S, Bhattacharyya D. Compression deformation of a biaxial stitched glass fibre reinforcement: Visualisation and image analysis using X-ray micro-CT. Composites: Part A, Applied Science and Manufacturing 2011;42(2):140-150.

[8] Bodig J, Jayne BA. Mechanics of Wood and Wood Composites. Malabar: Krieger, 1993.

[9] Haddad YM. Viscoelasticity of Engineering Materials. London: Chapman and Hall, 1995.

[10] Findley WN, Lai JS, Onaran K. Creep and Relaxation of Nonlinear Viscoelastic Materials, with an Introduction to Linear Viscoelasticity. Amsterdam: North-Holland, 1976.

[11] Kelly PA, Umer R, Bickerton S. Viscoelastic response of dry and wet fibrous materials during infusion processes. Composites Part A: Applied Science and Manufacturing 2006;37(6):868-873.

[12] Penneru AP, Jayaraman K, Bhattacharyya D. Viscoelastic behaviour of solid wood under compressive loading. Holzforschung 2006;60:294-298.

[13] Penneru AP. Characterisation and Mechanical Processing of Softened Wood. Unpublished doctoral thesis. New Zealand: The University of Auckland, 2007.

[14] Echaabi J, Nziengui MB, Hattabi M. Compressibility and relaxation models for fibrous reinforcements in liquid composites moulding. International Journal of Material Forming 2008;Suppl 1:851-854.

[15] Lee SH, Han JH, Kim SY, Youn JR, Song YS. Compression and relaxation behavior of dry fiber preforms for resin transfer molding. Journal of Composite Materials 2010;44(15):1801-1820.

Figure Captions

Fig. 1: Reinforcement materials: (a) Biaxial Stitched Fabric – top face (warp tows), (b) Biaxial Stitched Fabric – bottom face (weft tows), (c) Chopped Strand Mat, (d) Continuous Filament Mat, and (e) Plain Weave Fabric.

Fig. 2: BSF test results – (a) compaction and stress relaxation, (b) normalised stress relaxation response, and (c) comparison of peak and long term stresses.

Fig. 3: (a) Three component Maxwell element-based model using BSF data, and (b) schematic diagram of the five component Maxwell element-based model.

Fig. 4: Normalised curve plots for BSF 1, $v_f = 0.525$ (a) experimental and trial-fit curves, and (b) experimental and best-fit (model) curves.

Fig. 5: Sample normalised experimental and best-fit (model) curves for (a) CSM 3, $v_f = 0.42$, (b) CFM 3, $v_f = 0.415$, and (c) PWF 3, $v_f = 0.625$.

Fig. 6: Variation of model parameters with final fibre volume fraction for BSF – (a) stress constants, and (b) relaxation time constants.

Fig. 7: Variation of model parameters with final fibre volume fraction for CSM – (a) stress constants, and (b) relaxation time constants.

Fig. 8: Variation of model parameters with final fibre volume fraction for CFM – (a)

stress constants, and (b) relaxation time constants.

Fig. 9: Variation of model parameters with final fibre volume fraction for PWF – (a) stress constants, and (b) relaxation time constants.

Fig. 10: Normalised experimental and predicted stress-time curves for (a) BSF 2, ν_f = 0.55, and (b) BSF 5, ν_f = 0.625.

Fig. 11: Experimental and model predicted curves for (a) CFM 5, ν_f = 0.486, and (b) PWF 5, ν_f = 0.6.

Table 1: Specifications of reinforcement materials

Reinforcement	Nominal Areal Density (g/m^2)	Specifications	Manufacturer	Supplier
Biaxial Stitched Fabric (BSF)	820 (with stitching)	Biaxial 0º/90º reinforcement. 0º: 405.2 g/m^2; 90º: 399.4 g/m^2. Tows composed of E-glass fibres. Epoxy-polyester finish, stitched, 14 stitch rows per 25 mm of roll width. Dry thickness 0.686 mm. (Estimation: 9-10 fibre bundles per 25 mm of roll length.).	Vectorply Corporation Product Code: E-LT 2400-14P	High Modulus (NZ) Ltd. Product Code: EB820-1270
Chopped Strand Mat (CSM)	430	(Measured: Filament length 37-38 mm).	Owens Corning	Aurora Glass Fibre New Zealand
Continuous Filament Mat (CFM)	450	Filament is a bundle of Advantex® glass fibres. Single fibre diameter is 18.5 – 19 microns.	Owens Corning Product Code: M8610	Aurora Glass Fibre New Zealand
Plain Weave Fabric (PWF)	600	Warp: 111A 1200 tex Weft: 111A 600 tex Tow count: Warp: 27 per 100 mm Weft: 22 x 2 per 100 mm Rovings: 111 A, Owens Corning. 111A is a bundle of Advantex® glass fibres. Single fibre diameter is 18.5 – 19 microns.	Aurora Glass Fibre New Zealand	Aurora Glass Fibre New Zealand

Table 2: Test parameters and results for the stress relaxation experiments

Material and Test No.	Final Fibre Volume Fraction v_f	Final Thickness (mm)	No. of Layers	Comp Speed (mm/min)	Peak Stress (MPa)	Final Stress (MPa)	Final Stress (% of Peak Stress)	Stress Relax Time (s)
BSF 1	0.525	6.29	10	5.0	0.1798	0.1295	72.0	600
BSF 2*	0.55	6.07	10	5.0	0.2523	0.1822	72.2	600
BSF 3	0.575	5.77	10	5.0	0.4081	0.2961	72.6	600
BSF 4	0.6	5.39	10	5.0	0.5710	0.4196	73.5	600
BSF 5*	0.625	5.17	10	5.0	0.8373	0.6379	76.2	600
BSF 6	0.65	5.12	10	5.0	1.1569	0.9122	78.9	600
CSM 1	0.28	3.00	8	2.0	0.1649	0.0600	36.4	870
CSM 2	0.336	2.50	8	2.0	0.4177	0.1653	39.6	870
CSM 3	0.42	2.00	8	2.0	1.3601	0.9074	66.7	870
CSM 4	0.56	1.50	8	2.0	2.9992	2.5970	86.6	870
CFM 1	0.296	3.50	6	2.0	0.3908	0.2334	59.7	1620
CFM 2	0.346	3.00	6	2.0	0.7412	0.4808	64.9	1620
CFM 3	0.415	2.50	6	2.0	1.4744	1.0703	72.6	1620
CFM 4	0.519	2.00	6	2.0	2.7947	2.2525	80.6	1620
CFM 5*	0.486	3.41	10	5.0	1.7707	1.2691	71.7	600
PWF 1	0.55	3.16	8	2.0	0.1783	0.0756	42.4	1575
PWF 2	0.575	2.96	8	2.0	0.4231	0.2149	50.8	1575
PWF 3	0.625	2.78	8	2.0	0.5083	0.2795	55.0	1575
PWF 4	0.65	2.61	8	2.0	0.6751	0.4110	60.9	1575
PWF 5*	0.6	3.61	10	5.0	0.3899	0.2181	55.9	600

Notes:

(i) Sample size was 200 mm x 200 mm in every case.

(ii) A 0°/90°/0° lay-up was used for PWF.

(iii) Tests marked with an asterisk (*) were for model validation only and not used for model development.

Table 3: Best-fit model parameter values

Material & Test No.	Final Fibre ν_f	σ_0	σ_1	σ_2	τ_1	τ_2
BSF 1	0.525	0.7228	0.1974	0.0635	2.1227	117.4532
BSF 3	0.575	0.7282	0.1794	0.0677	2.6454	127.3347
BSF 4	0.6	0.7373	0.1672	0.0695	2.9590	131.3724
BSF 6	0.65	0.7899	0.1198	0.0637	4.6333	146.9843
CSM 1	0.28	0.3671	0.3219	0.2413	13.4384	205.3573
CSM 2	0.336	0.3991	0.3166	0.2165	12.7867	210.1112
CSM 3	0.42	0.6665	0.1700	0.1363	16.5636	249.5702
CSM 4	0.56	0.8646	0.0655	0.0597	20.7577	276.6250
CFM 1	0.296	0.5993	0.1969	0.1281	19.4381	408.0419
CFM 2	0.346	0.6504	0.1763	0.1192	18.8737	403.4681
CFM 3	0.415	0.7263	0.1387	0.0993	21.9072	458.4870
CFM 4	0.519	0.8047	0.0941	0.0799	27.4029	514.2936
PWF 1	0.55	0.4279	0.2704	0.1430	14.4354	364.3296
PWF 2	0.575	0.5114	0.2491	0.1309	14.6628	369.2843
PWF 3	0.625	0.5527	0.2271	0.1239	15.5388	381.1379
PWF 4	0.65	0.6110	0.1986	0.1122	16.7472	386.4296

Table 4: Normalised experimental and model stresses

Material & Test No.	Final Fibre Volume Fraction ν_f	Peak Stress		Final Stress		ΣResidual^2
		Expt	Model	Expt	Model	
BSF 1	0.525	1.0000	0.9837	0.7198	0.7232	0.0057
BSF 3	0.575	1.0000	0.9753	0.7257	0.7288	0.0061
BSF 4	0.6	1.0000	0.9740	0.7349	0.7380	0.0057
BSF 6	0.65	1.0000	0.9734	0.7885	0.7910	0.0035
CSM 1	0.28	1.0000	0.9033	0.3637	0.3702	0.0328
CSM 2	0.336	1.0000	0.9322	0.3958	0.4026	0.0304
CSM 3	0.42	1.0000	0.9728	0.6671	0.6707	0.0074
CSM 4	0.56	1.0000	0.9898	0.8659	0.8672	0.0009
CFM 1	0.296	1.0000	0.9243	0.5974	0.6017	0.02698
CFM 2	0.346	1.0000	0.9459	0.6488	0.6526	0.0191
CFM 3	0.415	1.0000	0.9643	0.7259	0.7292	0.0130
CFM 4	0.519	1.0000	0.9787	0.8060	0.8081	0.0053
PWF 1	0.55	1.0000	0.8413	0.4241	0.4298	0.0996
PWF 2	0.575	1.0000	0.8914	0.5081	0.5132	0.0770
PWF 3	0.625	1.0000	0.9037	0.5502	0.5547	0.0640
PWF 4	0.65	1.0000	0.9218	0.6088	0.6129	0.0465

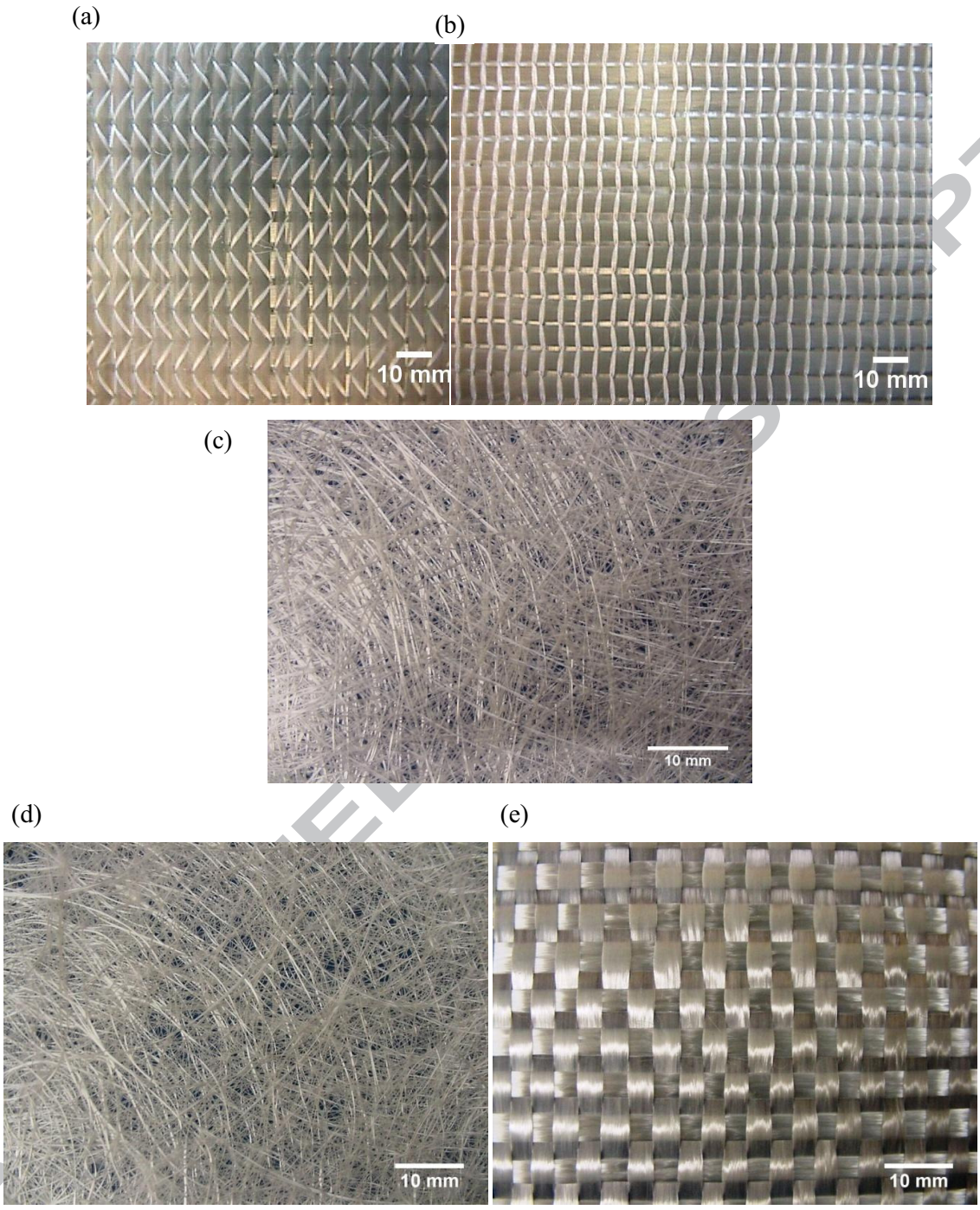

Fig. 1: Reinforcement materials: (a) Biaxial Stitched Fabric - top face (warp tows), (b) Biaxial Stitched Fabric - bottom face (weft tows), (c) Chopped Strand Mat, (d) Continuous Filament Mat, and (e) Plain Weave Fabric.

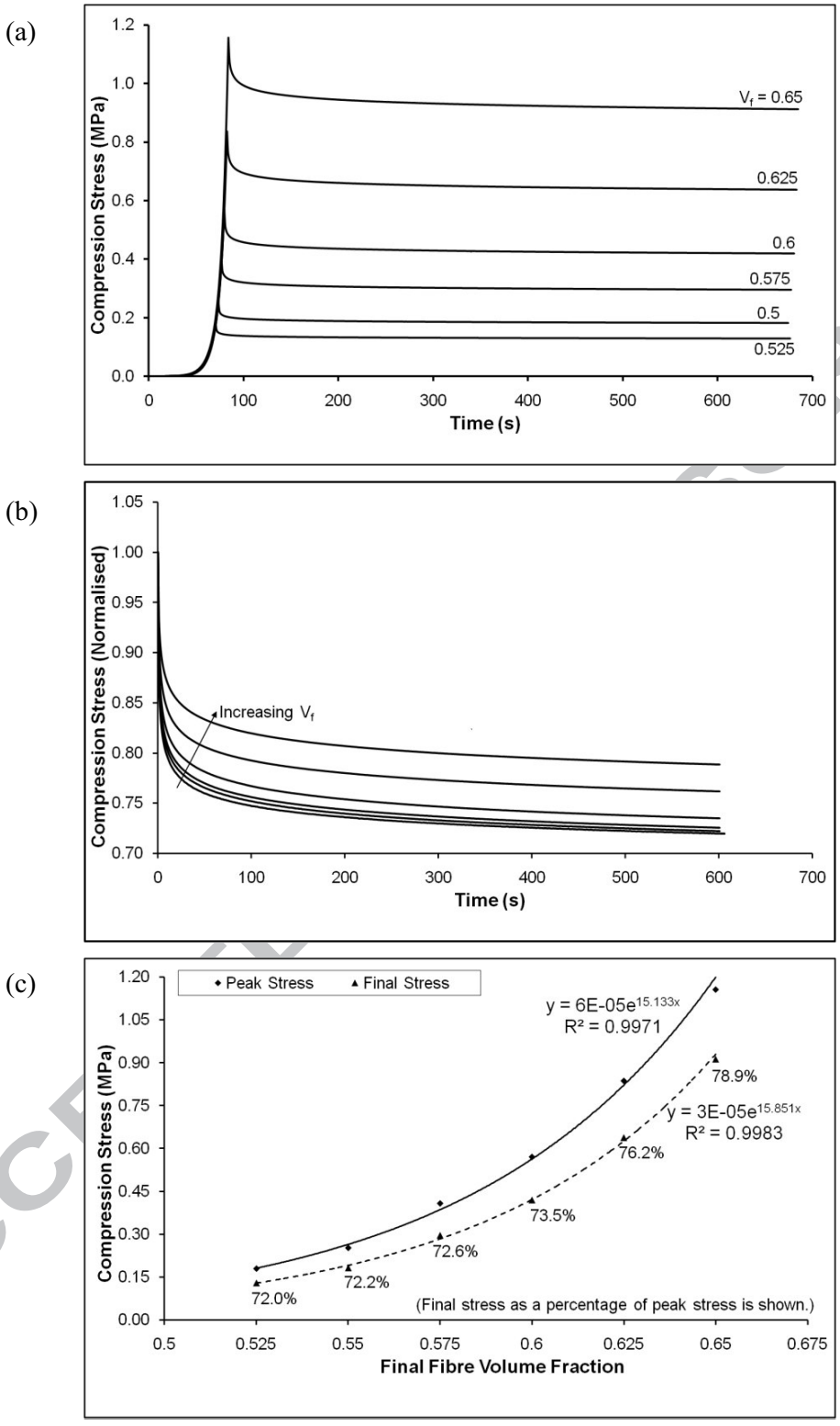

Fig. 2: BSF test results - (a) compaction and stress relaxation, (b) normalised stress relaxation response, and (c) comparison of peak and long term stresses.

(a)

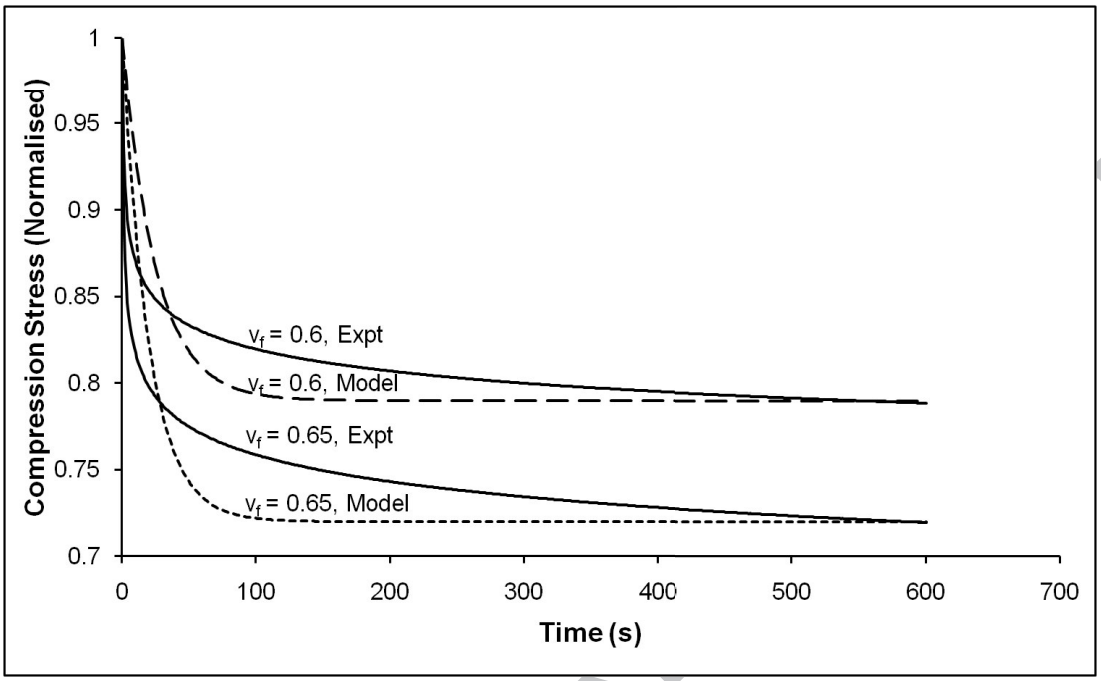

(b)

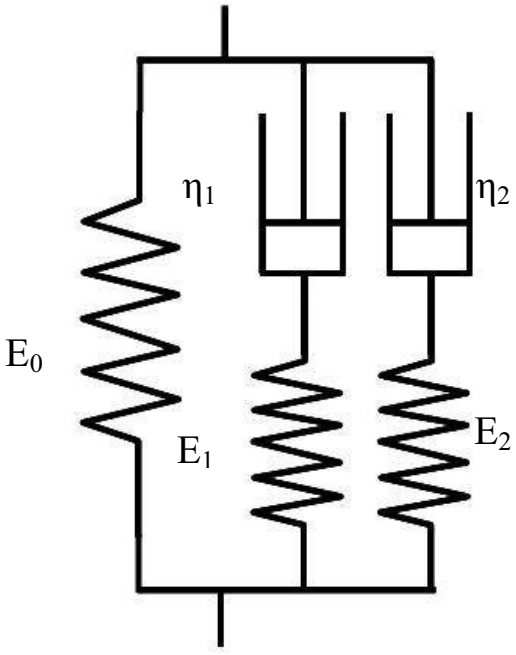

Fig. 3: (a) Three component Maxwell element-based model using BSF data, and (b) schematic diagram of the five component Maxwell element-based model.

(a)

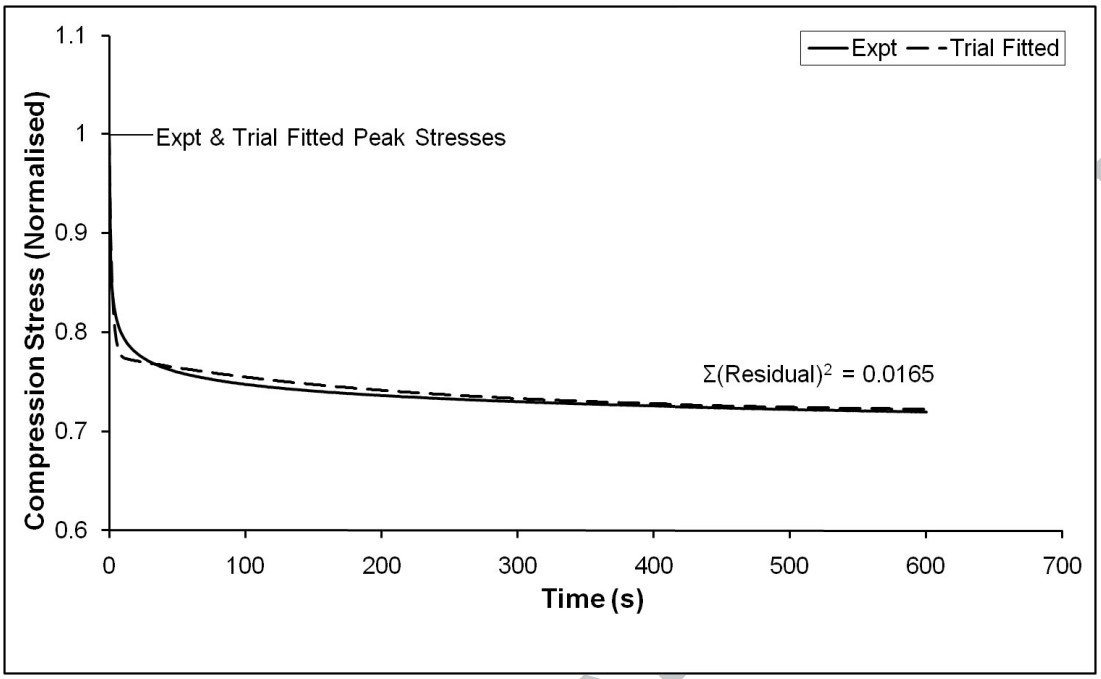

(b)

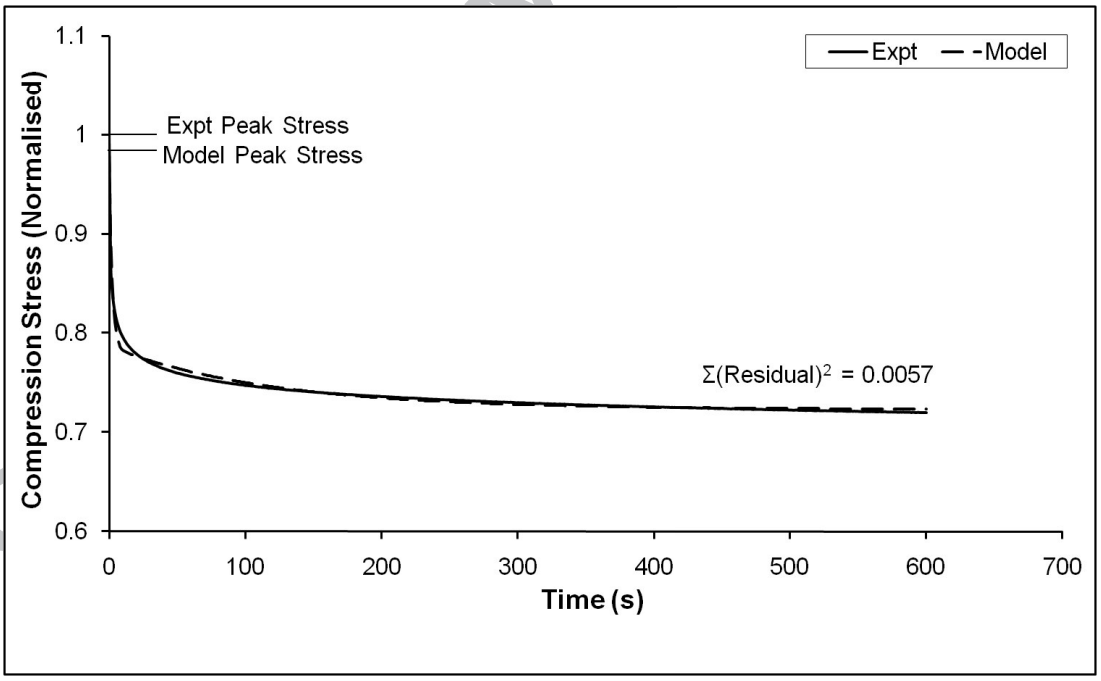

Fig. 4: Normalised curve plots for BSF 1, $\nu_f = 0.525$ (a) experimental and trial-fit curves, and (b) experimental and best-fit (model) curves.

(a)

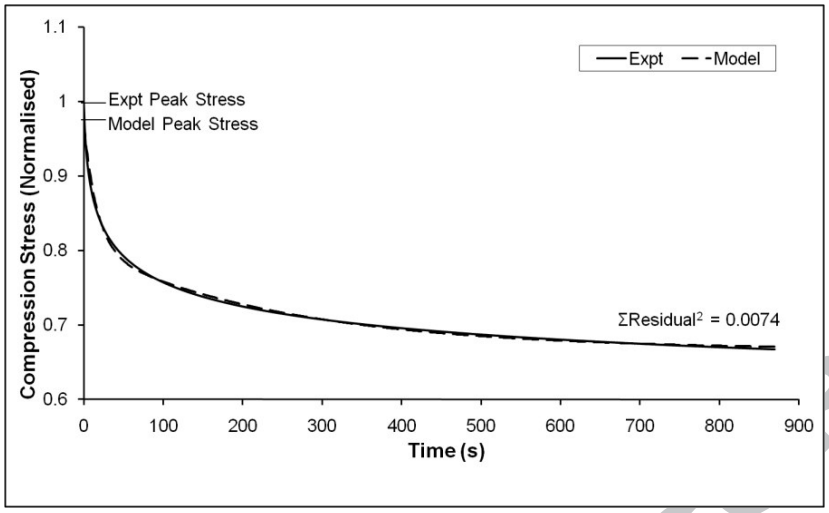

(b)

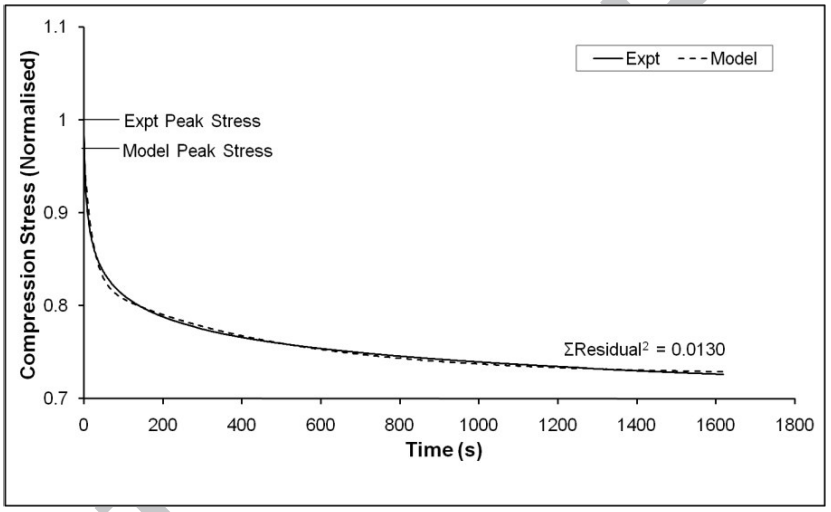

(c)

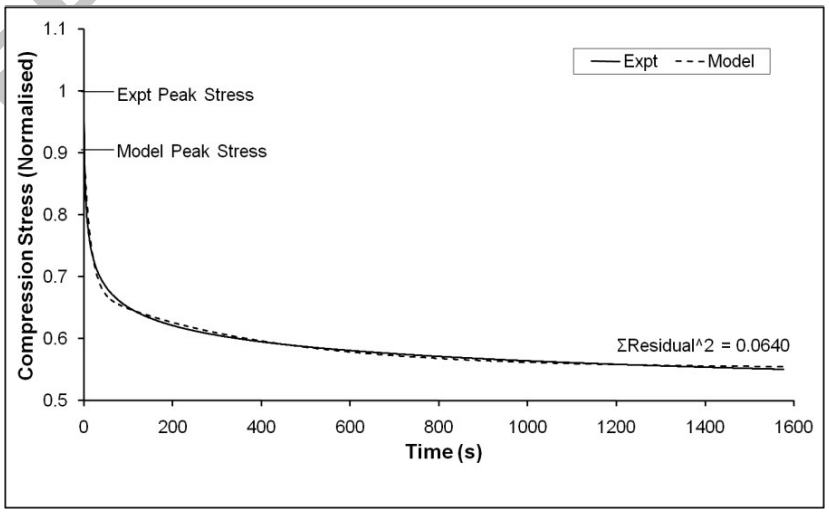

Fig. 5: Sample normalised experimental and best-fit (model) curves for (a) CSM 3, $\nu_f = 0.42$, (b) CFM 3, $\nu_f = 0.415$, and (c) PWF 3, $\nu_f = 0.625$.

(a)

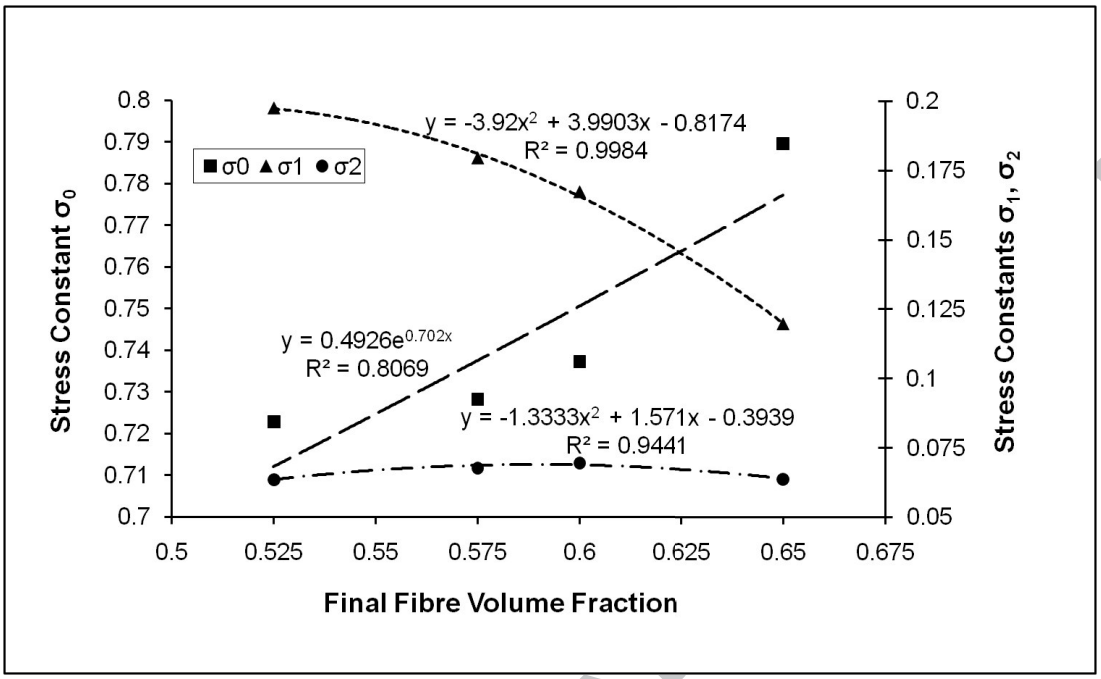

(b)

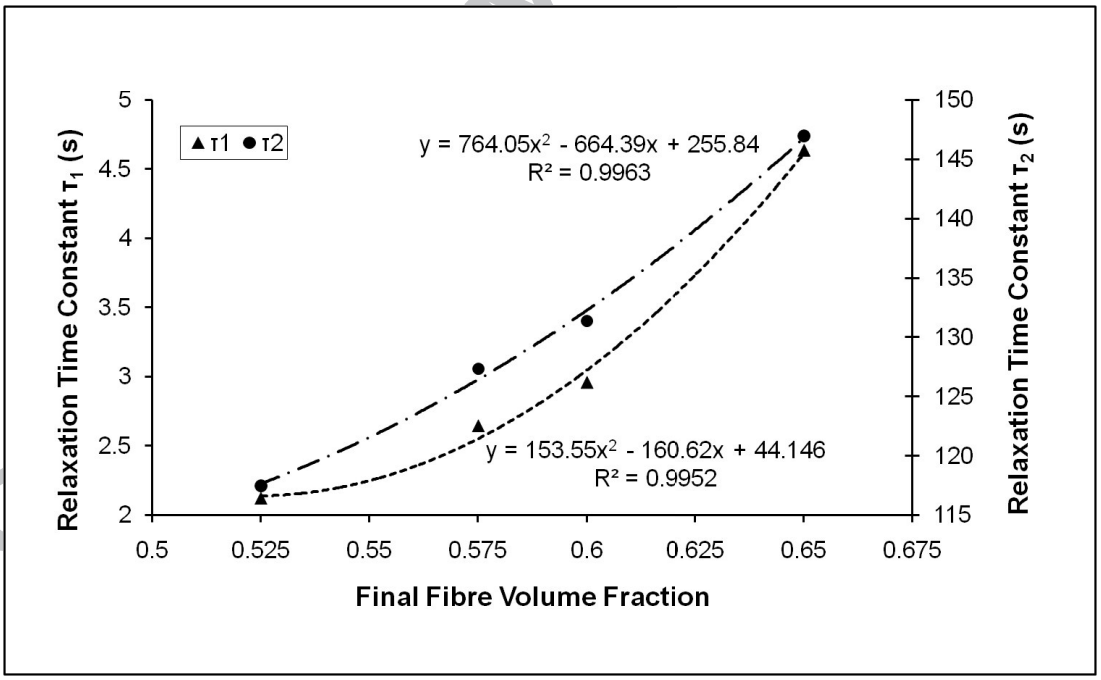

Fig. 6: Variation of model parameters with final fibre volume fraction for BSF – (a) stress constants, and (b) relaxation time constants.

(a)

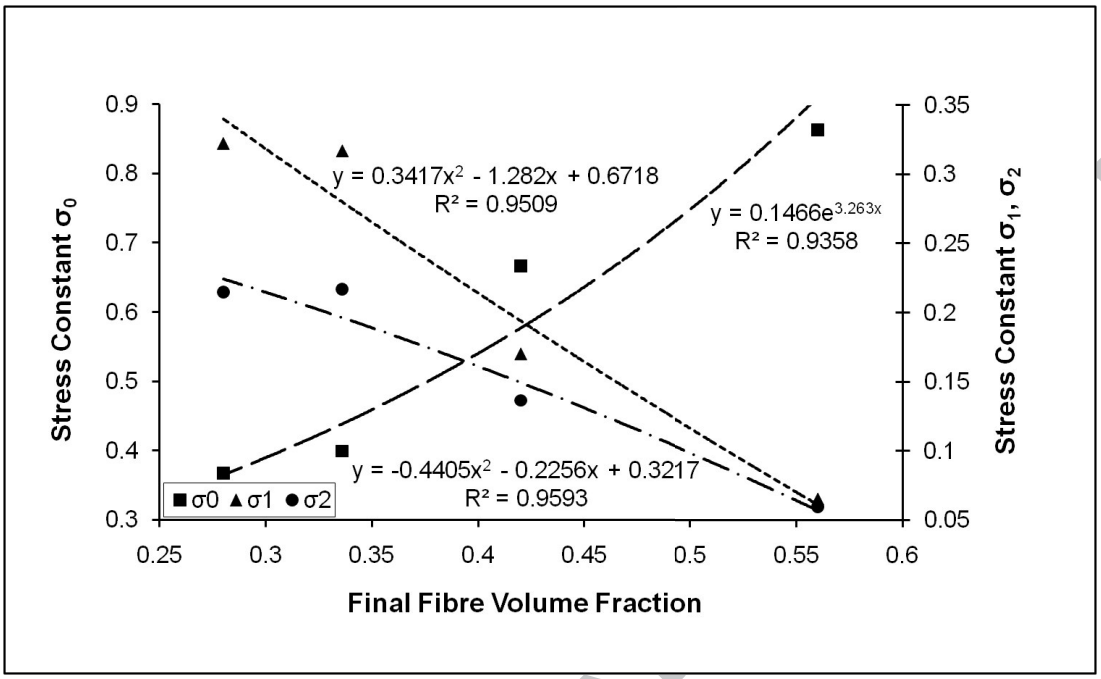

(b)

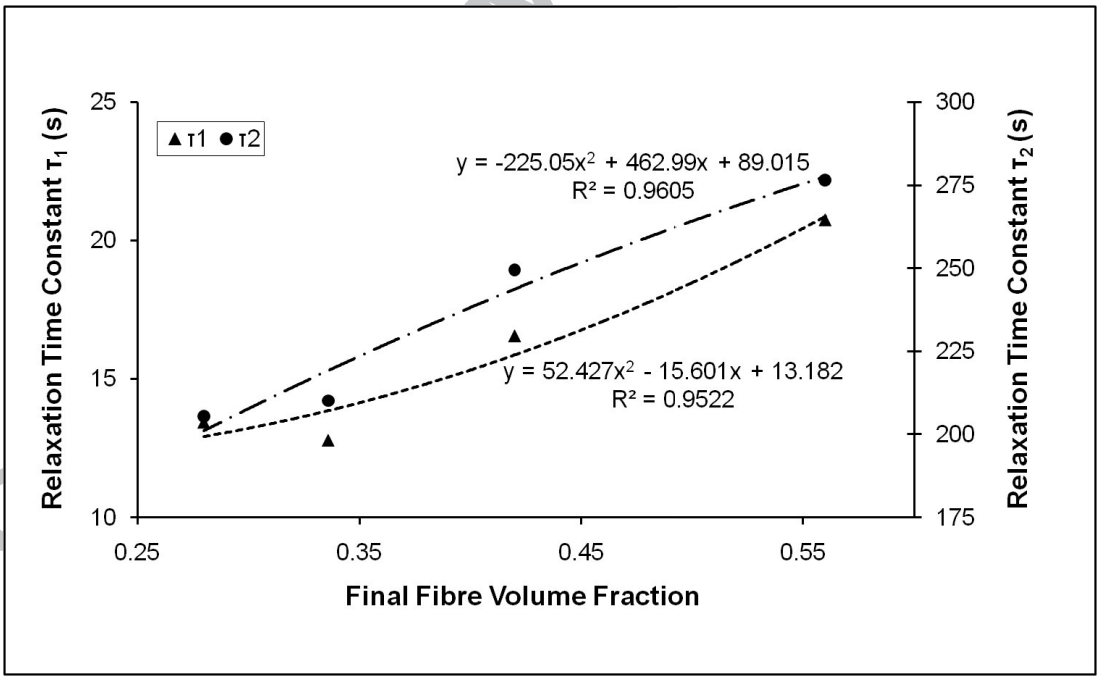

Fig. 7: Variation of model parameters with final fibre volume fraction for CSM – (a) stress constants, and (b) relaxation time constants.

(a)

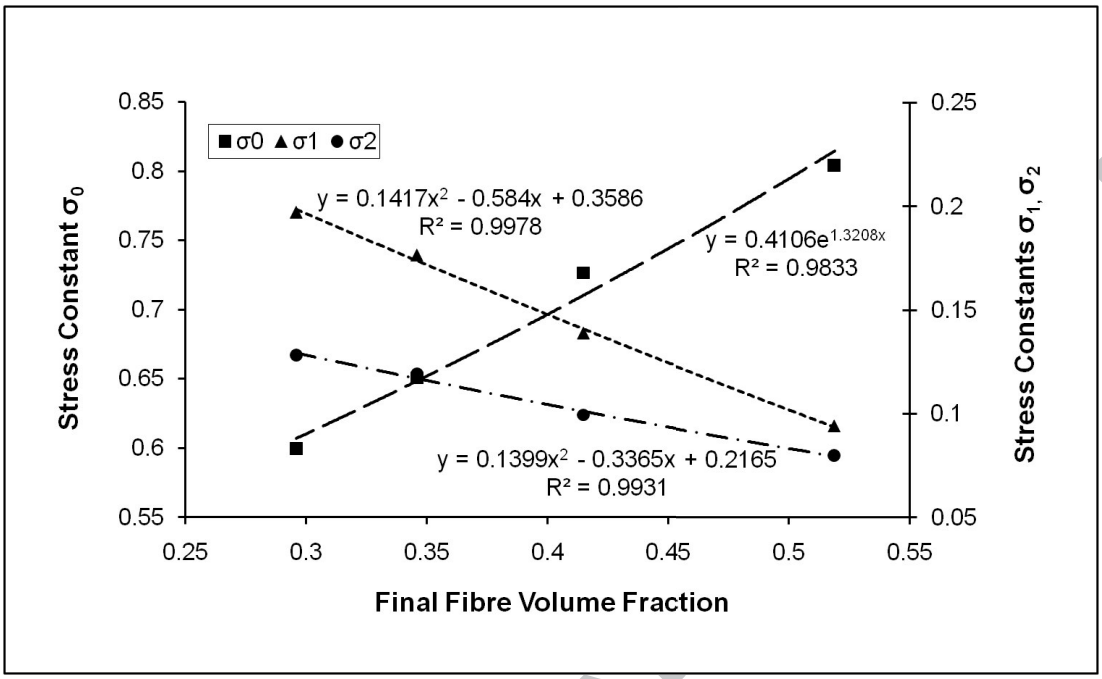

(b)

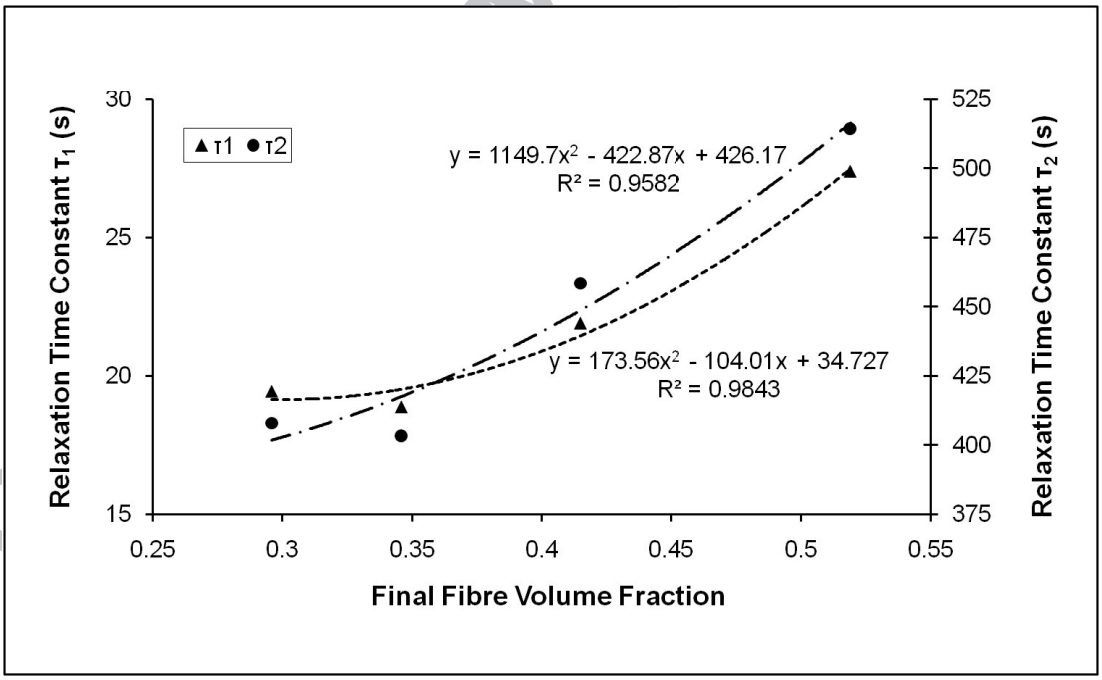

Fig. 8: Variation of model parameters with final fibre volume fraction for CFM – (a) stress constants, and (b) relaxation time constants.

(a)

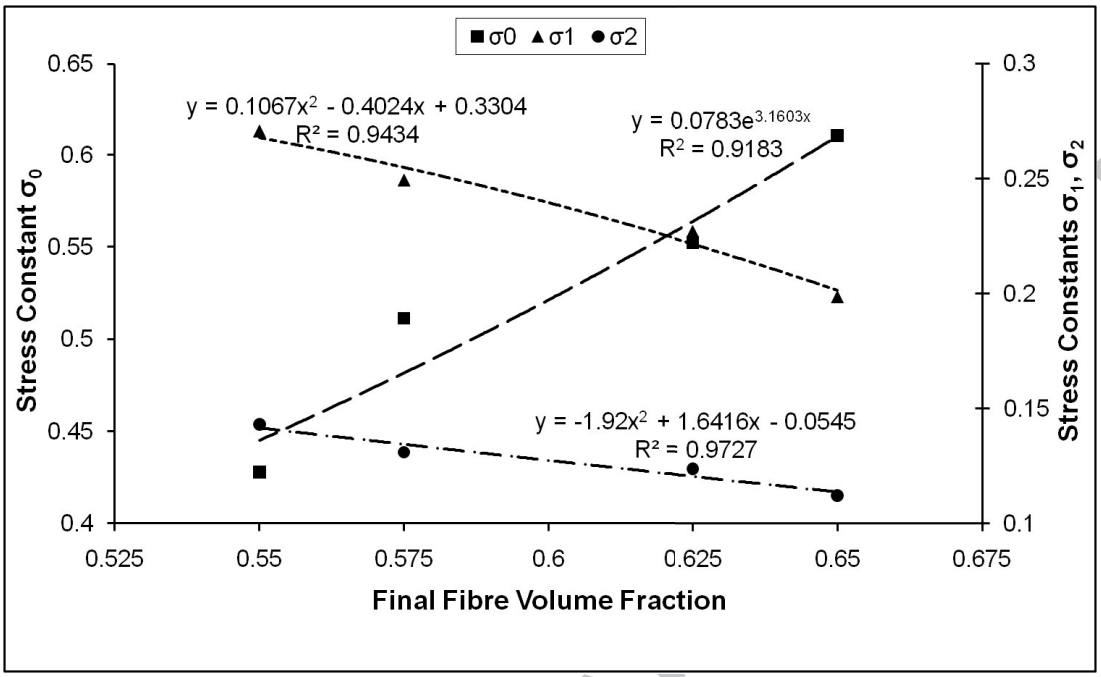

(b)

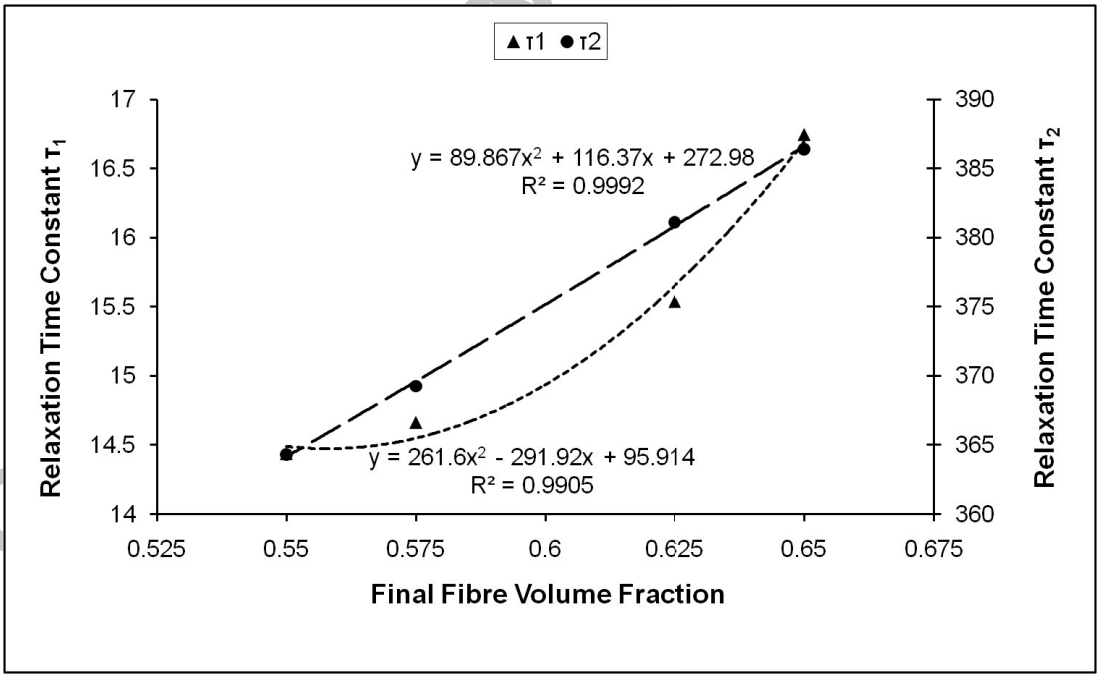

Fig. 9: Variation of model parameters with final fibre volume fraction for PWF – (a) stress constants, and (b) relaxation time constants.

(a)

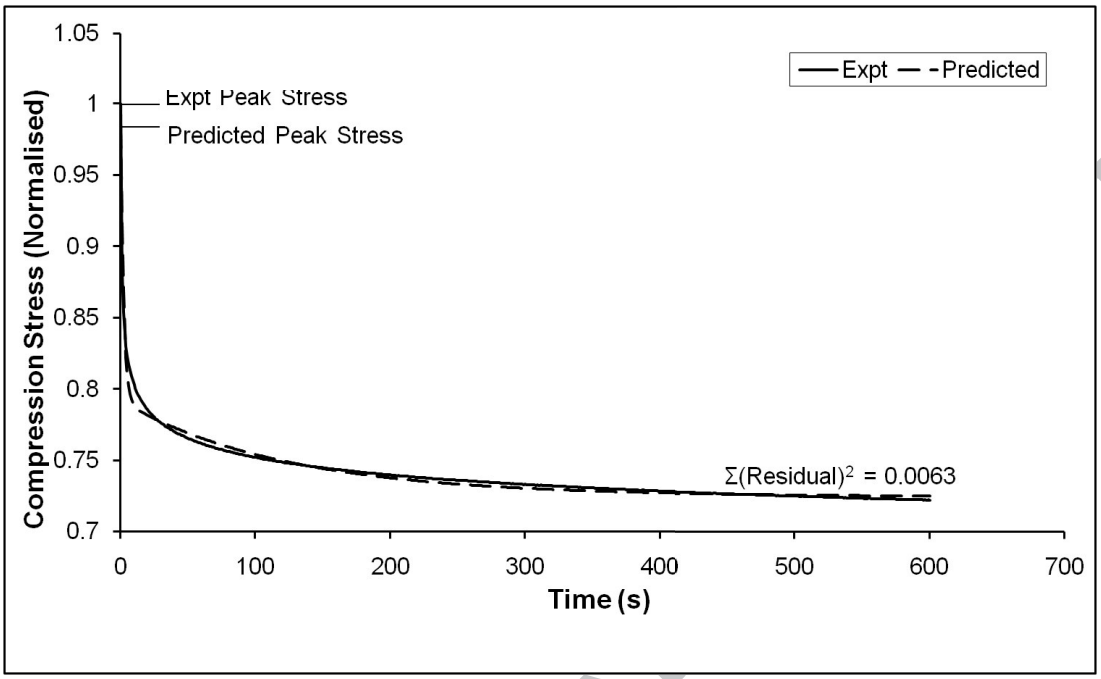

(b)

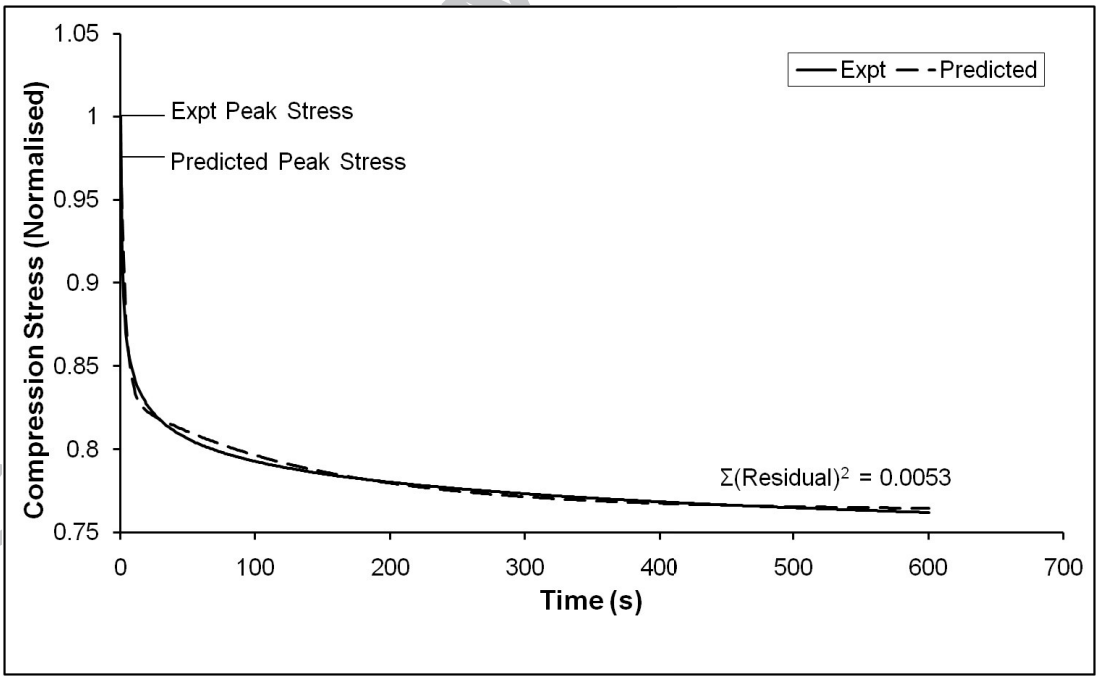

Fig. 10: Normalised experimental and predicted stress-time curves for (a) BSF 2, $\nu_f = 0.55$, and (b) BSF 5, $\nu_f = 0.625$.

(a)

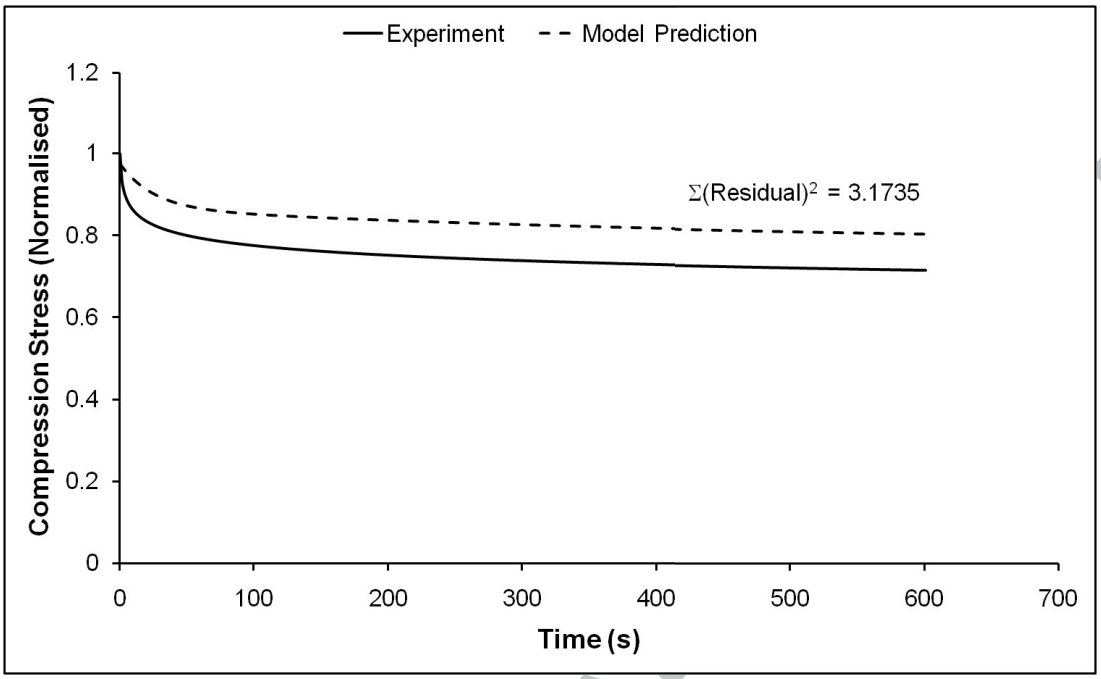

(b)

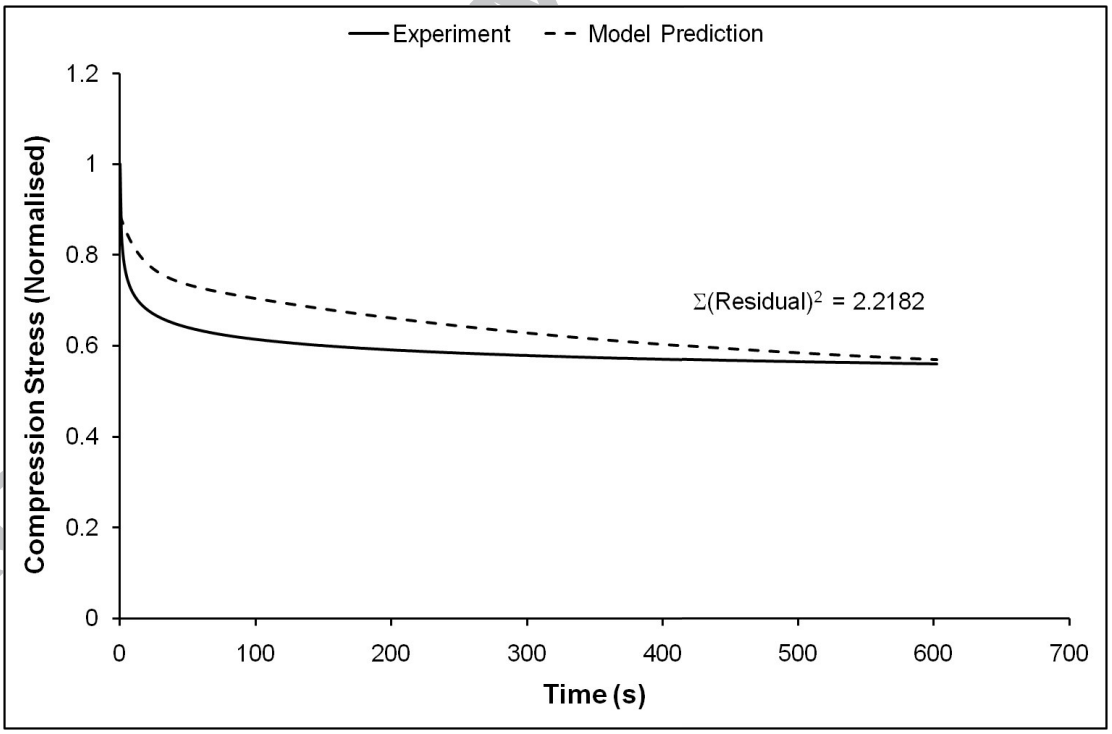

Fig. 11: Experimental and model predicted curves for (a) CFM 5, $\nu_f = 0.486$, and (b) PWF 5, $\nu_f = 0.6$.